EVALUATION OF THE PROTECTIVE EFFECTS OF ALPHA-LIPOIC ACID AGAINST ZINC OXIDE NANOPARTICLE-INDUCED PULMONARY INJURY IN RATS

Amira Ebrahim Alsemeh[1], Ebrahim Amin[1], Hend A. Yassin[2], Maha Eldousoky[3], Wafaa Mostafa[1], Amal AlShahat[1]

[1]Department of Human anatomy& Embryology, Faculty of Medicine, Zagazig University, Egypt
[2]Department of Medical Biochemistry, Faculty of Medicine, Alexandria University, Egypt
[3]Department of Basic Medical Sciences, College of Medicine, Taibah University, KSA

ABSTRACT

Background: Zinc oxide nanoparticles (ZnO-NPs) are broadly utilized due to their biocompatibility as well as broad applications. However, their toxicity, including hepatotoxicity, pulmonary toxicity, and neurotoxicity, has been reported in a concentration-dependent manner, primarily through oxidative stress. **Aim of the work:** This study sought to assess the protective role of alpha-lipoic acid (ALA) in mitigating pulmonary damage induced by zinc oxide nanoparticles (ZnO-NPs) in rats. **Material and methods:** A total of 28 rats were randomly assigned to four equal groups: control, Alpha-lipoic acid (ALA)-treated (200 mg/kg of ALA orally for three weeks), zinc oxide nanoparticles (ZnO-NP)-treated (single intraperitoneal injection of 1000 mg/kg) and ZnO-NPs+ALA groups. Lung tissue homogenates were analyzed for oxidative stress markers. Superoxide dismutase (SOD), Malondialdehyde (MDA), Glutathione peroxidase (GPX1), inflammatory cytokines Tumor necrosis factor alpha (TNF-α) Interleukin 6 (IL-6), and gene expression of fibrosis and immune response markers Natural cytotoxicity triggering receptor 3 (Ncr3), SMAD2 (SMAD Family Member 2), SMAD3 (SMAD Family Member 3), and SMAD7 (SMAD Family Member 7), Matrix Metallopeptidase 9 MMP9, Collagen coli-1A1 Col-1A1, Fibronectin, Monocyte chemoattractant protein-1 (MCP-1), transforming growth factor beta-1(TGF-β1), Interleukin 10(IL-10). Histopathological analysis was conducted using light microscopy, electron microscopy, and immunohistochemical techniques for alveolar macrophages (CD68) and nuclear factor-kappa B (NF-κB). **Results:** The results demonstrated that the ZnO-NPs + ALA group exhibited significantly higher SOD and GPX1 and lower MDA, TNF-α, and IL-6 levels compared to the ZnO-NPs group. Gene expression analysis demonstrated reduced expression of TGF-β1, Ncr3, SMAD2, SMAD3, MMP9, Col 1A1, Fibronectin, and MCP-1 in the ZnO-NPs + ALA group, whereas SMAD7 and IL-10 expression were elevated. **Conclusion:** It was demonstrated by our findings that ALA co-treatment effectively improved histopathological and ultrastructural changes in the lungs. Histomorphometric analysis revealed a significant downregulation of CD68 as well as NF-κB expression following ALA treatment. ALA effectively mitigates ZnO-NP-induced pulmonary injury by reducing oxidative stress, inflammation, and fibrosis-related gene expression, highlighting it as a promising protective agent against pulmonary damage caused by nanoparticles.

Keywords: *Zinc oxide nanoparticles, alpha lipoic acid, pulmonary toxicity, oxidative stress, fibrosis.*

Corresponding author: *Dr. Amira Ebrahim Alsemeh*
Email: dr.amira.alsemeh@gmail.com
ORCID: 0000-0002-5203-0784

INTRODUCTION

Nanotechnology is a promising, rapidly evolving discipline in scientific research worldwide concerned with using nanoparticles of ranging size from 1 to 100 nanometers ***(Fouad et al., 2021)***, with increasing Interest in the synthesis of metal as well as metal oxide nanoparticles ***(Amendola et al., 2020)***.

The zinc oxide nanoparticles (ZnO-NPs) are considered as one of the most commonly used oxide nanoparticles because of their excellent biocompatibility, low price, relatively low toxicity as well as their broad range of uses in photocatalysis, cosmetics, electronics, textile industry antimicrobial defense, drug delivery, cancer diagnosis, and management ***(Anjum et al., 2021; Fouad et al., 2021;Vasantharaj et al., 2021)***.

However, Toxicity, involving the liver, lung, neurons, and immune system has been reported, in a manner that is dependent on both concentration and time, under both in vitro and in vivo conditions through variable mechanisms of action. The primary mechanism of cytotoxicity is mediated by oxidative stress induced by the activity of zinc ions. Thus, the safe use of these particles at effective concentrations should be properly assessed ***(Keerthana and Kumar, 2020; Czyżowska and Barbasz, 2022)***.

The safety of ZnO-NPs along the years has been considered. The major routes of entry are inhalation, transdermal absorption/adsorption via the dermis and ingestion into the gastrointestinal tract ***(Chen et al., 2022)***. In toxicity studies, measured parameters, in addition to the ZnO-NPs distinct physicochemical properties, which differ according to their size, carried charge, surface functionalization, zeta potential, and morphology should be considered. The toxicity is globally estimated by the degree of morphological and molecular damage, like cell shrinkage of the cell, membrane destruction, increase of reactive oxygen species, oxidative stress, upregulation of heat shock proteins, changes in the permeability of cellular membranes, damage to cytoskeletal components, apoptotic changes, DNA damage, lysosomal affection, mitochondrial dysfunction, cytoplasm impairment, and other changes ***(Kad et al., 2022)***.

The lung is known to be more susceptible to oxidative damage than any other part in the body due to its continuous exposure to air which may contain hazardous particles or reactive gases, such as nitrogen oxides or ozone. Pulmonary oxidative stress is the result of the antioxidant capacity that becomes exhausted or depleted due to external factors, such as disrupted oxygen levels or air pollutants, or due to endogenous exposures. Oxidative stress effects on lung involve the activation of oxidase enzymes, lipid peroxidation, increased nitric oxide levels, and the induction of autophagy ***(Rogers and Cismowski, 2018)***. ZnO-NPs exposure successively results in lung oxidative stress and cell injury ***(Guo et al., 2022)***.

Alpha-lipoic acid (ALA), is a natural compound with both hydrophilic and hydrophobic properties, largely distributed in cells that can be synthesized by the human body in the liver, heart, and testis ***(Jan et al., 2015)***. It has multiple functions as it safeguards cellular membranes through its interaction with vitamin C as well as glutathione, which consequently recycles vitamin E. It also has a metal-chelating capability in addition to its role as a potent antioxidant. Physiologically, it is involved in the metabolism of glucose and lipids in addition to ATP production, acting as a cofactor for many enzymatic complexes in the mitochondria as Pyruvate dehydrogenase and α-ketoglutarate dehydrogenase enzymes ***(Wesselink et al., 2019; Deore et al., 2021)***. They are influenced by α-lipoic acid (ALA), which has been utilized as a racemic drug for alleviating pain and tingling sensations linked to diabetic polyneuropathy ***(Castro et al., 2019)***. ALA acts as a free radical scavenger, and its reduced form also neutralizes reactive oxygen species (ROS) ***(Packer and Cadenas, 2010)***. ALA holds therapeutic promise by aiding in glycemic regulation, preventing complications of diabetes, and potentially easing peripheral neuropathy symptoms. Additionally, it mitigates the toxicity of heavy metals, indicating its potential role in counteracting metal-induced toxicity ***(Henriksen, 2006; Salehi et al., 2019)***.

Additionally, its effectiveness in diseases like vascular disorders, hypertension, inflammatory and cardiovascular conditions, neurodegenerative disorders, autoimmune diseases, malignancy, and AIDS have been supported ***(Fenga et al., 2017)***.

THE AIM OF THE WORK

This study aims to assess the protective effects of alpha-lipoic acid (ALA) against pulmonary toxicity caused by zinc oxide nanoparticles (ZnO-NPs) in rats. Specifically, it seeks to assess the histopathological, biochemical, and immunohistochemical changes in lung tissues following ZnO-NP exposure and determine ALA's potential antioxidant and anti-inflammatory role in mitigating ZnO-NP-induced oxidative stress and cellular damage.

MATERIAL AND METHODS

Chemicals:

- Zinc oxide nanoparticles: identified by CAS No. 677450, were obtained as a fine, white powder in 5-gram bottles from Sigma Chemical Company, located on Eltayaran Street in Nasr City, Cairo, Egypt. The received powder had a particle size of less than 50 nm. A stock solution was prepared by suspending the ZnO-NPs in distilled water at a concentration of 500 mg/mL and homogenizing it using a vortex mixer for one minute (pH 7.3). A working solution with a concentration of 700 mg/mL was subsequently prepared following the method demonstrated by Mozaffari et al. (2015). This preparation process was conducted at the animal house of the Faculty of Medicine, Zagazig University, on 2018.2.1.

- Alpha lipoic Acid corrosive (Thiotacid or Thioctic acid) 300 mg cases were obtained from Eva-pharm pharmaceutical organization, Egypt**.**

Saline (0.9% sodium chloride solution) was supplied by the company of El-Nasr Pharmaceutical Chemicals (ADWIC), Egypt. ELISA kits were purchased from ELK (Wuhan) Biotechnology Co., Ltd., Hubei, China. All other chemicals used in the study were of analytical grade.

Animals and experimental design:

In this study, twenty-eight male albino rats weighing approximately 200-250 g were used. The rats were sourced from the Animal and Experimental House of the Faculty of Medicine at Zagazig University, Egypt. Prior to euthanasia, the animals were adapted to their environment for 7 days.

Ethical considerations: The study adhered to universal guidelines for the management, care, and utilization of rats in experimental studies. The rats had unrestricted access to water and a pellet diet, and were housed in metal cages under hygienic conditions with a standard light/dark cycle and a temperature of 22±2 °C. The experimental protocol was accepted by the Zagazig University Institutional Animal Care and Use Committee, (ZU-IACUC/3/F/31/20I8). All efforts were done to reduce animal suffering, and the procedures followed the National Guide for Care and Use of Laboratory Animals. The rats were randomly divided into four groups, each consisting of 7 rats:

Group I: control group: This group consisted of 7 rats, each receiving a single intraperitoneal injection of distilled water for three weeks.

Group II: Alpha lipoic Acid (ALA) group: This group included 7 rats, each receiving oral Alpha lipoic acid 200 mg/kg once daily for three weeks ***(Rasheed et al., 2012)***.

Group III: Zinc oxide nanoparticle (ZnO-NPs) group: This group included 7rats, each receiving a single intraperitoneal (IP) injection of Zinc oxide nanoparticles (1000 mg/kg) (as a single toxic dose in the experiment) ***(Ansari et al., 2015)*.**

Group IV: Zinc oxide nanoparticle (ZnO-NPs) group + ALA group: This group included 7rats, each receiving a single intraperitoneal (IP) injection of ZnO-NPs (1000 mg/kg) (as a single toxic dose) combined with ALA (200mg/kg) orally once daily for 3 weeks.

Ethical Consideration:

The experimental protocol received acceptance from the Zagazig University Institutional Animal Care and Use Committee *(ZU-IACUC/3/F/31/20I8).* Throughout the study, all efforts were dedicated to reduce animal suffering, adhering to the ARRIVE guidelines, the U.K. Animals (Scientific Procedures) Act of 1986, and the National Institutes of Health guide for the handling of laboratory animals (NIH Publications No. 8023, revised 1978) concerning experimental procedures.

Methods:

At 12:00 pm, exactly 24 hours following the final injection, all rats were humanely euthanized via a single intraperitoneal dose of sodium pentobarbital (60 mg/kg) ***(ICUC, 2014)***. Once death was confirmed, a thoracotomy was carried out and the lungs were carefully removed. The right lung was divided for different analyses: the first part was fixed in 10% neutral buffered formalin for light microscopy, while the second portion was immersed in 3% glutaraldehyde for electron microscopical examination. The left lung was also processed in parts: its initial section was homogenized to evaluate cytokine concentrations, antioxidant enzyme activities,

and lipid peroxidation levels, while the rest of the tissue was rapidly frozen using liquid nitrogen and stored at -80°C for subsequent gene expression studies.

Tissue sampling

Tissue samples were collected from the left-sided lungs to be immediately processed for light and electron microscopes. In addition, right-sided lung tissue samples were collected and stored at -80° C until they were processed for tissue homogenate preparation for biochemical markers analysis and gene expression studies.

Tissue homogenate preparation

For biochemical testing:

The lungs were homogenized on ice using RIPA buffer. The homogenates were then centrifuged at 10,000 g for 10 minutes at 4°C, and the supernatant was taken for further biochemical testing.

For gene expression:

RNA extraction was performed on the tissue using Trizol (Invitrogen; Thermo Fisher Scientific, Inc.) as per the manufacturer's guidelines. The supernatant was fully discarded, and the obtained RNA pellet was briefly air-dried. Subsequently, the RNA was dissolved in an appropriate amount of RNase-free water. A NanoDrop® ND–1000 Spectrophotometer (NanoDrop Technologies; Wilmington, Delaware, USA) was utilized to verify RNA quality and quantity.

Histological assessment

Light microscopic study:

For histopathological studies, after sacrificing the animals, Lung tissues were immersed in 10% neutral-buffered formalin for fixation for a period of 48 hours. Following fixation, the samples underwent dehydration through a graded ethanol series, cleared in xylene, and subsequently embedded in paraffin wax blocks. Serial sections (3-5 µm thick) were cut using a microtome, transferred to a water bath, and then dried in an oven for waxing. The sections were stained with haematoxylin and eosin. Following staining, the tissue sections on the slides were placed on slides with Di-N-Butyl Phthalate Xylene (DPX) as the mounting medium and sealed with coverslips. All prepared slides were subsequently examined using a light microscope ***(Mozaffari et al., 2015; Suvarna et al., 2018)***.

Electron microscopic study:

The specimens were promptly immersed in 2.5% glutaraldehyde prepared in 0.1 mol/L cacodylate buffer (pH 7.3) for 4 hours, followed by post-fixation in 1% osmium tetroxide in the same buffer for an additional 2 hours.

After fixation, the samples underwent dehydration through a graded ethanol series, cleared with xylene, and then embedded in paraffin wax blocks. Semi-thin (1 µm) sections were prepared and stained with toluidine blue to identify suitable areas for ultrathin sectioning. Ultrathin sections (60–80 nm) were prepared, stained using 2% of uranyl acetate and 2% of lead citrate, and analyzed under EM ***(Hayat, 1973)***.

Immunohistochemical Analysis for Assessing Alveolar Macrophages (CD68) and Nuclear Factor kappa B (NF-κB) Proteins

Formalin-fixed, paraffin-embedded lung tissue specimens were processed for immunohistochemical analysis. The avidin–biotin–peroxidase method was employed to detect alveolar macrophages (CD68) and the expression of Nuclear Factor Kappa B (NF-κB). All samples underwent standard processing. Paraffin sections (4 µm thick) were deparaffinized in xylene, rehydrated through graded ethanol, and incubated with 0.3% H_2O_2 for 30 minutes to prevent endogenous peroxidase activity.

Antigen retrieval was performed by heating the sections in citrate buffer (pH 6) using a microwave for 15 minutes. To minimize non-specific binding, the sections were treated with 10% goat serum for 30 minutes. Following a gentle PBS wash, the tissue sections were incubated overnight at 4 °C with primary antibodies: a rat monoclonal anti- NF-κB antibody (1:500 dilution, Transduction Laboratories, San Diego, California, USA) and a mouse monoclonal anti-CD68 antibody (1:200 dilution, code NCL-L-CD68; Leica Biosystems, Benton La, Newcastle Ltd, UK).

The slides were subsequently counterstained with Sections stained with Mayer's hematoxylin, dehydrated, and mounted using

DPX. Negative controls were prepared by excluding the primary antibody during incubation. Positive immunoreactivity for CD68 and NF-κB was identified microscopically by the presence of a characteristic brown coloration in the immunoreactive cells ***(Ramos-Vara, 2010; Taylor, 2014; Sanderson et al., 2018)***.

Biochemical assessment

Superoxide Dismutase (SOD), Malondialdehyde (MDA), Glutathione peroxidase 1 (GPX1), tumor necrosis factor alpha (TNF –α), interleukin (IL) – 6

Enzyme-Linked Immunosorbent Assay kits were used to quantify the concentrations of SOD, MDA, GPX1, TNF-α, and IL-6 in the homogenate following the assay kit methodology Catalog Numbers. (CUSABIO, USA) CSB-E08555r, CSB-E11987r, and CSB-E04640r ***(Abd El Fadil et al., 2020)***.

Gene expression of apoptotic markers by quantitative real-time-polymerase chain reaction (qRT-PCR):

A High-Capacity cDNA Reverse Transcription Kit (Applied Biosystems™, USA) was employed for the synthesis of cDNA. The reverse transcription reaction mixture was incubated at 45 °C for 60 minutes, and the enzyme was subsequently inactivated by heating to 85 °C for 10 minutes using a Biometra 96-well thermal cycler (Applied Biosystems). The resulting cDNA product was stored at −20 °C until it was needed for subsequent polymerase chain reaction (PCR).

Real-time RT-PCR was conducted using the Mx3005P Real-Time PCR System (Agilent Stratagene, USA) with TOPreal™ qPCR 2X PreMIX (SYBR Green with low ROX) (Cat. # P725 or P750) (Enzynomics, Korea), following the manufacturer's guidelines and the assay protocol ***(Khamis et al., 2019; Khamis et al., 2020; Khamis et al., 2021)***. The thermal cycling protocol consisted of an initial denaturation at 95°C for a duration of 12 minutes, followed by 40 cycles comprising denaturation at temperature of 95°C for 20 seconds, annealing at 60°C for 30 seconds duration, and extension at 72°C for 30 seconds. The sequence-specific oligonucleotide primers were designed by Sangon Biotech, Beijing, China.

Primer sequences:

Natural cytotoxicity triggering receptor 3 (Ncr3) F: 5′-TCCTCAACAAGCCTCCAACG-3′ and R: 5′- CGTGACAGAGACATTTGCCC-3′.SMAD2 F:5′-CAAACGTGCACAGGTGACAG-3′ and R:5′- GACTGGCGTTGGAAGAAGGA-3′. SMAD3 F:5′-CTGGGCAAGTTCTCCAGAGTT-3′ and R: 5′- AAGGGCAGGATGGACGACAT-3′. SMAD7 F:5′-GAGTCTCGGAGGAAGAGGCT-3′ and R: 5′- CTGCTCGCATAAGCTGCTGG-3′. Mmp9 F:5′-GATCCCCAGAGCGTTACTCG-3′ and R: 5′- GTTGTGGAAACTCACACGCC-3′. Collagen coli-1 F:5′-GCAATGCTGAATCGTCCCAC-3′ and R: 5′- CAGCACAGGCCCTCAAAAAC-3′. Fibronectin F:5′-GGATCCCCTCCCAGAGAAGT-3′ and R: 5′- GGGTGTGGAAGGGTAACCAG-3′. MCP-1 F:5′-TAGCATCCACGTGCTGTCTC-3′ and R: 5′- CAGCCGACTCATTGGGATCA-3′. TGF- β1 F:5′-AGGGCTACCATGCCAACTTC-3′ and R: 5′- CCACGTAGTAGACGATGGGC-3′. IL-10 F:5′- GCTCAGCACTGCTATGTTGC-3′ and R: 5′-TTGTCACCCCGGATGGAATG-3′. GAPDH F:5′-GCATCTTCTTGTGCAGTGCC-3′ and R: 5′-GGTAACCAGGCGTCCGATAC-3′.

RNA concentration was quantified based on the threshold cycle (Ct) values obtained during PCR. Messenger RNA (mRNA) target gene expression levels were normalized to the mRNA levels of glyceraldehyde-3-phosphate dehydrogenase (GAPDH), which acted as an internal control using the 2-ΔΔCT method ***(Livak and Schmittgen, 2001)***.

Histomorphometric measurement

The percentage of the area occupied by CD68-immunostained cells and NF-κB immuno-expression was quantified in 10 randomly selected, non-overlapping microscopic fields per slide at 400× magnification. This analysis was conducted on a single lung specimen.

Histomorphometric measurements were performed using an image analysis system (Leica Qwin 500 software, Image Computer System Ltd., Cambridge, England) at the Department of Anatomy and Embryology, Zagazig University

Statistical Analysis:

The data collected were analyzed using the IBM SPSS software package, version 20 *(Armonk, NY, USA),* and presented as the mean±SD. Statistical analysis was performed using ANOVA and Tukey's post hoc test for pairwise comparisons. A p-value of ≤0.05 indicated significant relations.

RESULTS

Biochemical analysis

Oxidative stress markers

Rats exposed to ZnO-NPs exhibited elevated oxidative stress, evidenced by significantly (P<0.05) higher malondialdehyde (MDA) levels and reduced activity of the antioxidant enzymes Glutathione peroxidase 1 (GPX1) and superoxide dismutase (SOD) in cerebellar tissues compared to the control group (P<0.001). As illustrated in **tables (1, 2, 3)** respectively, co-treatment with ALA led to an improvement in oxidative balance, demonstrated by a reduction in MDA levels and an increase in GPX1 and SOD activity compared to ZnO-NPs group (P<0.001) but still revealed significant differences from the control and ALA groups. Meanwhile, insignificant differences were found between the control and ALA groups.

Inflammatory mediators

Rats exposed to ZnO-NPs showed a significant increase in cerebellar levels of Interleukin-6 (IL-6) and Tumor Necrosis Factor-alpha (TNF-α) compared to the control and ALA-treated groups. Co-administration of ALA markedly reduced the ZnO-NP-induced elevation of IL-6. A similar trend was observed with TNF-α levels, which were significantly lower in the ALA co-treatment group than in the ZnO-NPs group, although they remained significantly higher than those in the control and ALA-only groups. No significant differences were detected between the control and ALA groups. These findings are detailed in **tables (4, 5)**.

Gene Expression of the Transforming growth factor beta (TGF-β), Natural cytotoxicity triggering receptor 3 (Ncr3) gene, SMAD2, SMAD3, Matrix metalloproteinase 9 (MMP9), collagen type I (Col 1A1), Fibronectin, monocyte chemoattractant protein-1 (MCP1)

Regarding the results of the expression of TGF-β, Ncr3, SMAD2, SMAD3, MMP9, Col 1A1, Fibronectin, and MCP1 genes, significantly higher expression was shown in the ZnO-NPs treated group as compared to other experimental groups. Interestingly, significantly lower expression was shown in the ZnO-NPs +ALA treated group compared to the ZnO-NPs treated group. However, still this level of expression was significantly higher than control and ALA groups (P<0.001). No statistical difference was demonstrated among the control and ALA groups. As shown in **tables (6, 7, 8, 9, 10, 11, 12, 13)**.

Gene Expression of SMAD7, Interleukin 10 (Il-10)

Regarding the results of the SMAD7 and Interleukin 10 (Il-10) genes expression levels, it was found that the ZnO-NPs treated group had significantly lower levels than all other experimental groups. In contrast, the ZnO-NPs +ALA treated group had a significantly lower level than the ZnO-NPs treated group **(Table 14, 15)**.

Histological study

Light microscopic examination

Hematoxylin and eosin stain (H&E)

No significant biochemical differences were observed between the control and ALA-treated groups; therefore, they were grouped together as a single control group for histological analysis.

Histological examination of lung sections stained with H&E demonstrated that the control group exhibited normal spongy lung architecture. The alveoli appeared open, variably sized, and polygonal, separated by thin interalveolar septa. Alveolar ducts and sacs were visible, and well-structured bronchioles were interspersed among the alveoli. Bronchioles of various sizes displayed intact, folded mucosal linings, encircled by organized smooth muscle fibers and outer adventitia **(Figure 1a)**.

Higher magnification of the highlighted area in Figure 1a revealed that the alveoli were lined by a single layer of two cell types: flat, squamous cells with flattened nuclei (type I pneumocytes) and cuboidal cells with rounded nuclei (type II pneumocytes) **(Figure 1b)**.

In contrast, the lungs of the ZnO-NP-exposed group showed pronounced alveolar damage, characterized by widespread alveolar collapse, intense infiltration of inflammatory cells, and congestion with increased thickness of the walls of pulmonary blood vessels **(Figure 2a)**.

At higher magnification **(Figure 2b)**, the selected area from Figure 2a revealed thickened interalveolar septa and collapsed alveoli, with signs of interstitial consolidation.

In the group co-treated with ALA and ZnO-NPs, the lung histology showed substantial improvement, closely resembling that of the control group **(Figure 3a)**.

However, at higher magnification **(Figure 3b)**, mild thickening of some interalveolar septa, a few collapsed alveoli, and slightly thickened blood vessels were still detected in certain areas.

Mallory's trichrome stain (MT)

Figures (4a–c) illustrate Masson's trichrome (MT)-stained lung sections from the different experimental groups. In the control group, collagen fibers appeared as fine strands primarily located within the narrow interalveolar septa, and around pulmonary blood vessels and bronchioles **(Figure 4a)**. In contrast, lungs from the ZnO-treated group displayed a marked increase in collagen deposition, with dense fibers prominently surrounding bronchioles, blood vessels, and throughout the interstitial tissue **(Figure 4b)**. However, pretreatment with ALA prior to ZnO exposure noticeably reduced both the density and spread of collagen fibers in these regions, as shown in **figure (4c)** Morphometric and statistical evaluations of collagen fiber distribution confirmed a significant increase in the ZnO-only group compared to the untreated controls, while the ZnO+ALA group exhibited a significant reduction in collagen content **(Figure 4d)**.

Electron microscopic examination

Transmission electron microscopy of lung tissue from the control group revealed open alveolar spaces lined by two distinct types of cells. Type I pneumocytes had flattened nuclei, while type II pneumocytes featured rounded, euchromatic nuclei and cytoplasm rich in lamellar bodies—some fully formed, others appearing empty—as well as short apical microvilli. The interalveolar septa were thin and contained a single capillary **(Figures 5a, b)**.

In contrast, the ZnO-treated group exhibited ultrastructural abnormalities, including markedly thickened interalveolar septa filled with numerous interstitial cells displaying pleomorphic nuclei and multiple congested capillaries **(Figures 6a, b)**. Co-administration of ALA with ZnO significantly improved these pathological changes **(Figsures 7a, b)**.

Examination of the air-blood barrier in control lungs showed its typical trilaminar structure: a thin extension of type I pneumocyte cytoplasm, the fused basal laminae of the pneumocyte and endothelial cell, and the capillary endothelial cytoplasm **(Figure 8a)**. However, in the ZnO-exposed group, the air-blood barrier was disrupted, showing irregular, swollen cytoplasm in both type I pneumocytes and endothelial cells (Fig. 8b). In the ALA + ZnO group, the structure of the air-blood barrier appeared nearly normal, with only minor cytoplasmic swelling in type I pneumocytes **(Figure 8c)**.

Immuno-histological examination

Alveolar macrophage CD68 immuno-staining

Figure 9 (a-c) shows immunohistochemical staining for alveolar macrophage CD68 in lung tissues from various experimental groups. In the control group, only a few cells displayed faint brown cytoplasmic staining **(Figure 9a)**. The ZnO-treated group showed a marked increase in the number of cells with strong positive cytoplasmic staining **(Figure 9b)**. In contrast, the ZnO+ALA group exhibited fewer cells with brown cytoplasmic staining **(Figure 9c)**. Morphometric and statistical analysis of the percentage area of CD68 immuno-expression revealed a significant increase in the ZnO-treated group compared to controls. In the ZnO+ALA

group, the percentage area of CD68 expression was significantly reduced compared to the ZnO-only group (P<0.05), as shown in **figure (9d)**.

NF-κB immuno-staining

Figure 10 (a-c) shows immunohistochemical staining for NF-κB in lung tissue from different experimental groups. In the control group, only a few alveolar cells exhibited a faint positive brown reaction **(Fig. 10a).** In contrast, the ZnO-treated group displayed a strong positive brown cytoplasmic staining in several alveolar cells **(Figure 10b)**.

The lungs of the ALA-treated group before ZnO exposure showed fewer alveolar cells with positive brown staining **(Figure 10c)**. Morphometric and statistical analysis confirmed that the ZnO-treated group had significantly higher NF-κB immunostaining compared to the untreated control group. In the ZnO+ALA group, the NF-κB immuno-expression was significantly reduced compared to the ZnO-only group (P<0.05), as seen in the figure (**Figure 10d)**.

Table (1): Superoxide Dismutase SOD (U/mg) among all studied groups.

Group		Control Group	ALA Group	ZnO Group	ZnO+ALA Group
x̄ ± SD		208.34±6.70	209.3±7.13	77.13±8.61	192.37±18.37
Range		202-220	200-223	64-90	171.6-220
F		210.67			
P		<0.001**			
Post hoc	+veC		0.87 NS	<0.001**	0.008*
	ALA			<0.001**	0.005*
	ZnO				<0.001**

N=7 rats x̄: mean Sd: Standard deviation F: ANOVA test Post hoc: Least Significant Difference (LSD)
*NS: Non significant (P>0.05) *: Significant (P<0.05) **: Highly significant (P<0.001).*

Table (2): Malondialdehyde MDA (nmol/mg) among all studied groups.

Group		Control Group	ALA Group	ZnO Group	ZnO+ALA Group
x̄ ± SD		0.71±0.29	0.9±0.29	7.24±1.35	2.05±0.25
Range		0.4-1.3	0.5-1.2	5-9	1.7-2.4
F		127.27			
P		<0.001**			
Post hoc	+veC		0.57 NS	<0.001**	0.001*
	ALA			<0.001**	0.003*
	ZnO				<0.001**

N=7 rats x̄: mean Sd: Standard deviation F: ANOVA test Post hoc: Least Significant Difference (LSD)
*NS: Non significant (P>0.05) *: Significant (P<0.05) **: Highly significant (P<0.001).*

Table (3): Glutathione peroxidase 1 GPX (U/mg) among all studied groups.

Group		Control Group	ALA Group	ZnO Group	ZnO+ALA Group
x̄ ± SD		226.11±21.89	219.5±21.56	89.17±5.31	127.83±3.88
Range		202-265	203-266	80-95	45-51
F		101.29			
P		<0.001**			
Post hoc	+veC		0.48 NS	<0.001**	<0.001**
	ALA			<0.001**	<0.001**
	ZnO				<0.001**

N=7 rats x̄: mean Sd: Standard deviation F: ANOVA test Post hoc: Least Significant Difference (LSD)
*NS: Non significant (P>0.05) *: Significant (P<0.05) **: Highly significant (P<0.001).*

Table (4): Tumor necrosis factor alpha TNF (pg/mg) among all studied groups.

Group		Control Group	ALA Group	ZnO Group	ZnO+ALA Group
x̄ ± SD		49.46±1.63	47.83±2.34	586.96±8.95	170.26±12.91
Range		47-52	44-50	575-600	150-190
F		7320.84			
P		<0.001**			
Post hoc	+veC		0.68 NS	<0.001**	<0.001**
	ALA			<0.001**	<0.001**
	ZnO				<0.001**

N=7 rats x̄: mean Sd: Standard deviation F: ANOVA test Post hoc: Least Significant Difference (LSD)
*NS: Non significant (P>0.05) *: Significant (P<0.05) **: Highly significant (P<0.001).*

Table (5): Interleukin– 6 Il-6 (pg/mg) among all studied groups.

Group		Control Group	ALA Group	ZnO Group	ZnO+ALA Group
x̄ ± SD		50.03±5.28	48.91±5.65	439.8±13.03	68.57±16.76
Range		40-60	42-59	420-460	50-100
F		1888.16			
P		<0.001**			
Post hoc	+veC		0.85 NS	<0.001**	0.002*
	ALA			<0.001**	0.001*
	ZnO				<0.001**

N=7 rats x̄: mean Sd: Standard deviation F: ANOVA test Post hoc: Least Significant Difference (LSD)
*NS: Non significant (P>0.05) *: Significant (P<0.05) **: Highly significant (P<0.001).*

Table (6): Transforming growth factor beta (TGFb) among all studied groups.

Group		Control Group	ALA Group	ZnO Group	ZnO+ALA Group
x̄ ± SD		1.08±0.16	0.97±0.16	4.12±0.31	1.55±0.57
Range		0.85-1.2	0.85-1.23	3.7-4.5	0.7-2.23
F		133.97			
P		<0.001**			
Post hoc	+veC		0.51 NS	<0.001**	0.007*
	ALA			<0.001**	0.001*
	ZnO				<0.001**

N=7 rats x̄: mean Sd: Standard deviation F: ANOVA test Post hoc: Least Significant Difference (LSD)
*NS: Non significant (P>0.05) *: Significant (P<0.05) **: Highly significant (P<0.001).*

Table (7): Natural cytotoxicity triggering receptor 3 (NCr3) among all studied groups.

Group		Control Group	ALA Group	ZnO Group	ZnO+ALA Group
x̄ ± SD		0.96±0.30	0.79±0.28	5.8±0.55	1.5±0.5
Range		0.54-1.3	0.6-1.4	5-6.5	0.9-2.11
F		208.17			
P		<0.001**			
Post hoc	+veC		0.42 NS	<0.001**	0.01*
	ALA			<0.001**	0.002*
	ZnO				<0.001**

N=7 rats x̄: mean Sd: Standard deviation F: ANOVA test Post hoc: Least Significant Difference (LSD)
*NS: Non significant (P>0.05) *: Significant (P<0.05) **: Highly significant (P<0.001).*

Table (8): Mothers Against Decapentaplegic homolog 2 (SMAD2) among all studied groups.

Group		Control Group	ALA Group	ZnO Group	ZnO+ALA Group
x̄ ± SD		1.19±0.20	1.04±0.24	5.26±0.55	1.63±0.66
Range		0.8-1.3	0.75-1.35	4.5-6	0.7-2.56
F		128.48			
P		<0.001**			
Post hoc	+veC		0.53 NS	<0.001**	0.05*
	ALA			<0.001**	0.02*
	ZnO				<0.001**

N=7 rats x̄: mean Sd: Standard deviation F: ANOVA test Post hoc: Least Significant Difference (LSD)
*NS: Non significant (P>0.05) *: Significant (P<0.05) **: Highly significant (P<0.001).*

Table (9): Mothers Against Decapentaplegic homolog 3 (SMAD3) among all studied groups.

Group		Control Group	ALA Group	ZnO Group	ZnO+ALA Group
x̄ ± SD		1.06±0.2	0.92±0.21	3.75±0.49	1.45±0.41
Range		0.7-1.3	0.71-1.29	3-4.5	0.7-1.87
F		93.44			
P		<0.001**			
Post hoc	+veC		0.41 NS	<0.001**	0.04*
	ALA			<0.001**	0.005*
	ZnO				<0.001**

N=7 rats x̄: mean Sd: Standard deviation F: ANOVA test Post hoc: Least Significant Difference (LSD)
*NS: Non significant (P>0.05) *: Significant (P<0.05) **: Highly significant (P<0.001).*

Table (10): Matrix metalloproteinase 9 (MMP9) among all studied groups.

Group		Control Group	ALA Group	ZnO Group	ZnO+ALA Group
x̄ ± SD		1.07±0.08	1.00±0.15	6.76±0.66	1.58±0.54
Range		0.95-1.13	0.7-1.1	6-7.5	0.8-2.14
F		263.43			
P		<0.001**			
Post hoc	+veC		0.76 NS	<0.001**	0.03*
	ALA			<0.001**	0.02*
	ZnO				<0.001**

N=7 rats x̄: mean Sd: Standard deviation F: ANOVA test Post hoc: Least Significant Difference (LSD)
*NS: Non significant (P>0.05) *: Significant (P<0.05) **: Highly significant (P<0.001).*

Table (11): Collagen type I (Col1) among all studied groups.

Group		Control Group	ALA Group	ZnO Group	ZnO+ALA Group
x̄ ± SD		0.92±0.12	0.87±0.21	1.9±0.84	1.43±0.31
Range		0.8-1.11	0.5-1.2	0.9-3.31	1.2-2.1
F		8.11			
P		<0.001**			
Post hoc	+veC		0.84 NS	<0.001**	0.03*
	ALA			<0.001**	0.02*
	ZnO				0.04*

N=7 rats x̄: mean Sd: Standard deviation F: ANOVA test Post hoc: Least Significant Difference (LSD)
*NS: Non significant (P>0.05) *: Significant (P<0.05) **: Highly significant (P<0.001).*

Table (12): Fibronectin among all studied groups.

Group		Control Group	ALA Group	ZnO Group	ZnO+ALA Group
x̄ ± SD		1.26±0.23	1.12±0.22	6.29±0.73	1.86±0.23
Range		0.95-1.65	0.91-1.5	5-7	1.5-2.11
F		235.16			
P		<0.001**			
Post hoc	+veC		0.51 NS	<0.001**	0.007*
	ALA			<0.001**	0.001*
	ZnO				<0.001**

N=7 rats x̄: mean Sd: Standard deviation F: ANOVA test Post hoc: Least Significant Difference (LSD)
*NS: Non significant (P>0.05) *: Significant (P<0.05) **: Highly significant (P<0.001).*

Table (13): Monocyte chemoattractant protein-1 (MCP1) among all studied groups.

Group		Control Group	ALA Group	ZnO Group	ZnO+ALA Group
x̄ ± SD		1.23±0.25	1.02±0.31	4.48±0.65	1.68±0.47
Range		0.83-1.62	0.78-1.6	3.5-5.15	0.9-2.21
F		86.02			
P		<0.001**			
Post hoc	+veC		0.35 NS	<0.001**	0.05*
	ALA			<0.001**	0.006*
	ZnO				<0.001**

N=7 rats x̄: mean Sd: Standard deviation F: ANOVA test Post hoc: Least Significant Difference (LSD)
*NS: Non significant (P>0.05) *: Significant (P<0.05) **: Highly significant (P<0.001)*

Table (14): Mothers Against Decapentaplegic homolog 7 (SMAD7) among all studied groups.

Group		Control Group	ALA Group	ZnO Group	ZnO+ALA Group
x̄ ± SD		1.2±0.19	1.28±0.22	0.44±0.27	0.83±0.19
Range		1.01-1.54	0.99-1.55	0.18-0.8	0.6-1.2
F		17.96			
P		<0.001**			
Post hoc	+veC		0.50 NS	<0.001**	0.003*
	ALA			<0.001**	0.001*
	ZnO				0.002*

N=7 rats x̄: mean Sd: Standard deviation F: ANOVA test Post hoc: Least Significant Difference (LSD)
*NS: Non significant (P>0.05) *: Significant (P<0.05) **: Highly significant (P<0.001)*

Table (15): Interleukin– 10 Il-10 among all studied groups.

Group		Control Group	ALA Group	ZnO Group	ZnO+ALA Group
x̄ ± SD		1.33±0.35	1.42±0.47	0.3±0.07	0.85±0.34
Range		0.98-2.01	0.8-2	0.2-0.4	0.5-1.5
F		.	12.37		
P		<0.001**			
Post hoc	**+veC**		0.54 NS	<0.001**	0.02*
	ALA			<0.001**	0.003*
	ZnO				0.007*

N=7 rats x̄: mean Sd: Standard deviation F: ANOVA test Post hoc: Least Significant Difference (LSD)
*NS: Non significant (P>0.05) *: Significant (P<0.05) **: Highly significant (P<0.001).*

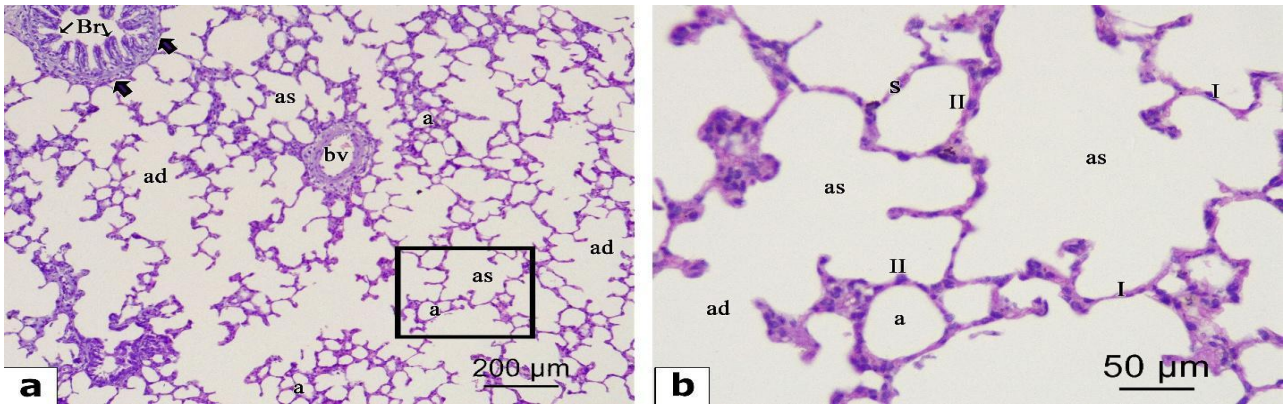

Figure (1): *Representative microscopic images of H&E-stained lung sections from the control group.* ***(a, b):*** *reveals medium sized bronchiole (Br) with folded lining respiratory epithelium (thin arrows) which are regularly arranged around smooth muscles (thick arrows), alveolar duct (ad), alveolar sac (as), alveoli (a), blood vessel (bv), thin septum (s), pneumocyte I (I)and pneumocyte II (II)* ***[a= 200 µm x100, b = 50 µm x400].***

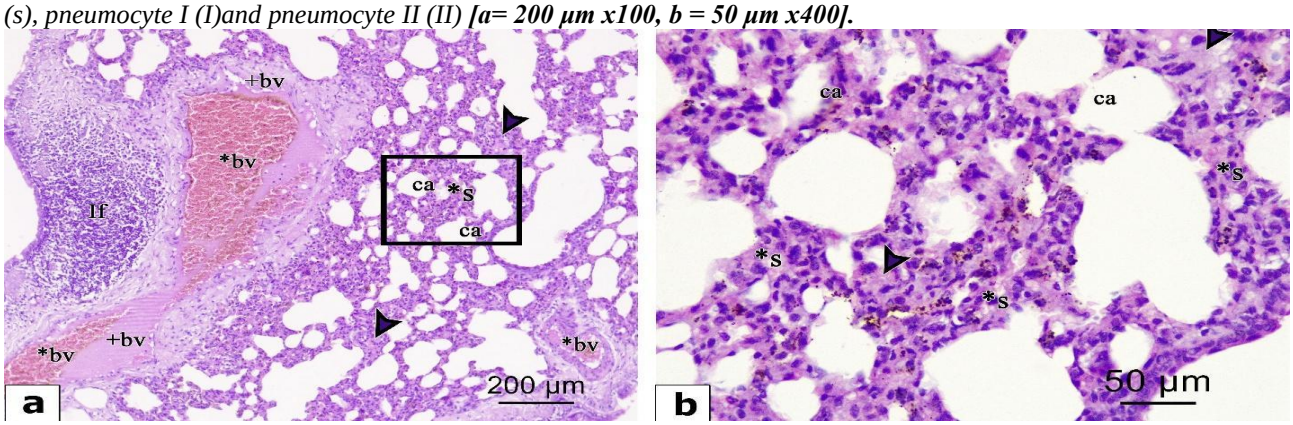

Figure (2): *Representative microscopic images of H&E-stained lung sections from the ZnO-treated experimental group.* ***(a, b)*** *shows collapsed alveoli (ca), thick septum(*s), consolidation (arrowhead), thick wall blood vessel (+bv), vascular congestion(*bv) and extensive prei bronchial cellular infiltration (IF).* ***[a= 200 µm x100, b = 50 µm x400]****.*

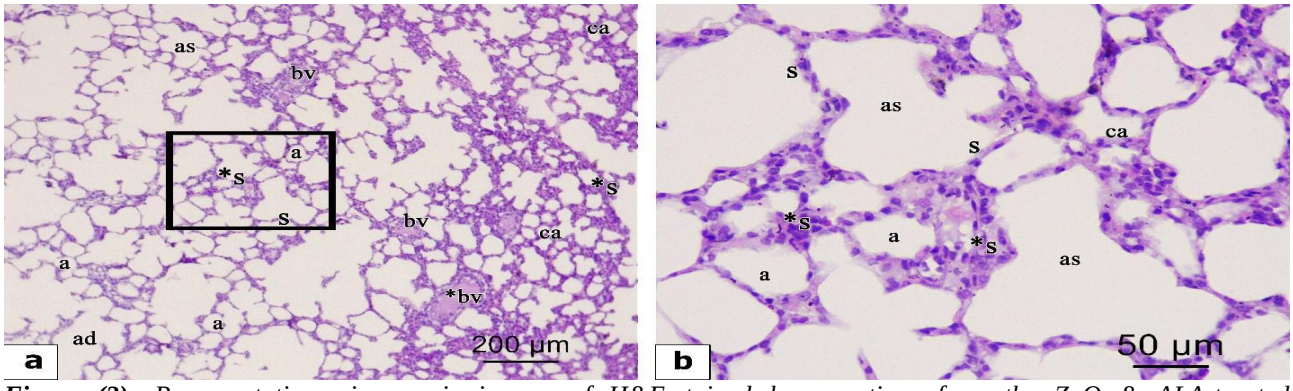

Figure (3): *Representative microscopic images of H&E-stained lung sections from the ZnO & ALA-treated experimental group.* ***a,b)*** *show thin septum (s) , alveoli (a), alveolar sac (as), alveolar duct (ad) and blood vessels (bv). Few thick septa (*s), few collapsed alveoli (ca), and congested blood vessels can be observed (*bv).* ***[a= 200 µm x100, b = 50 µm x400]****.*

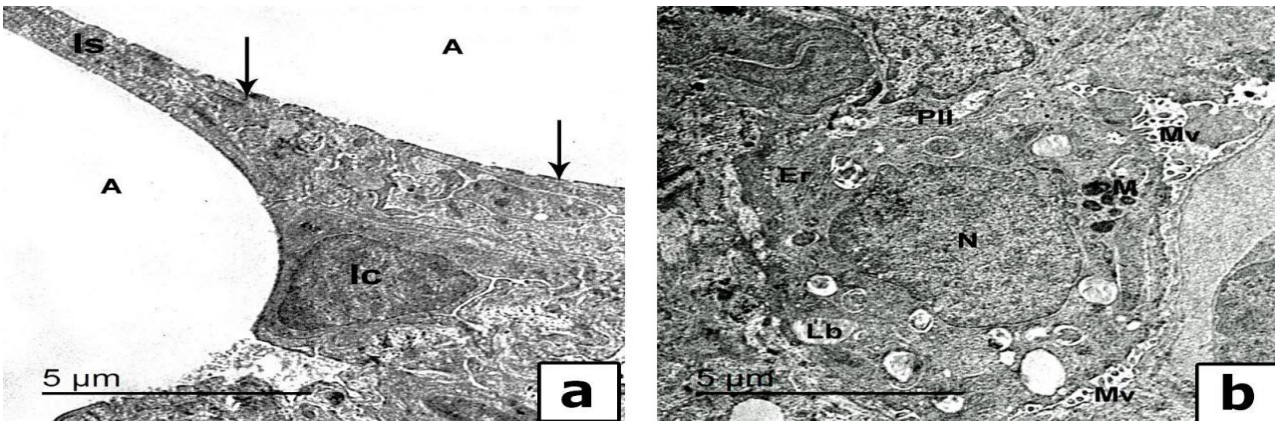

Figure (4): *An electron micrograph of ultrathin sections from the experimental control group I displays:* ***(a)*** *patent alveoli (A), thin interalveolar septum (Is), and interstitial cell (Ic). A thin or attenuated cytoplasm of type pneumocyte (arrow) is noticed.* ***(b)*** *showing type II pneumocyte (PII) with few short microvilli (Mv) on its surface, euchromatic nucleus (N), characteristic lamellar bodies (Lb) and small mitochondria (M) and some rough endoplasmic reticulum (Er).* ***[a, b scale bar=5 µm].***

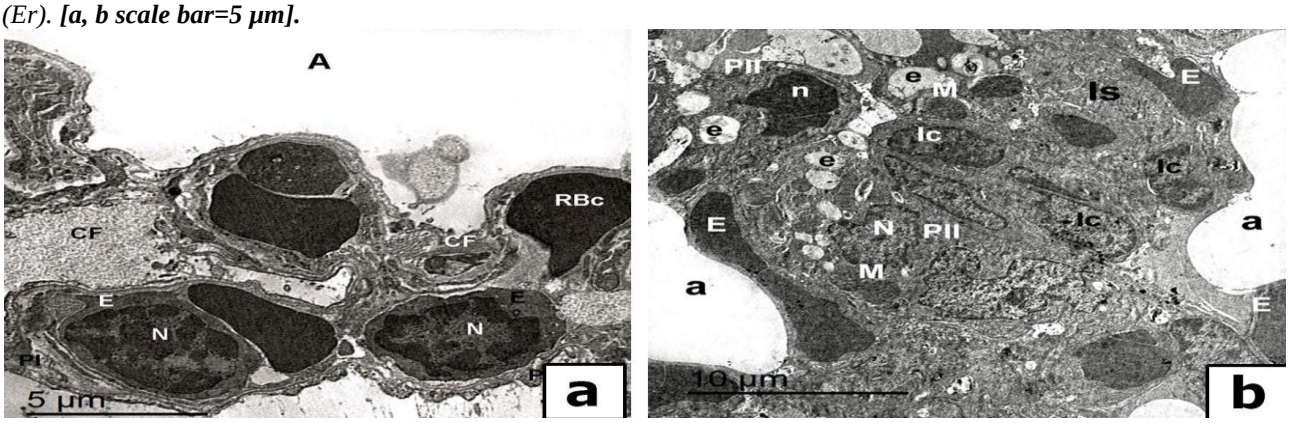

Figure (5): *An electron micrograph of ultrathin sections of experimental ZNO treated group shows* ***(a)*** *a part of interalveolar septum adjacent to alveoli (A) with deposition of some collagen fibers in longitudinal and transvers sections (CF). Numerous congested blood capillaries (E) show rounded indented nuclei with clumps of heterochromatins (N) and red blood cells (RBCs) in their lumens, in (b) collapsed alveoli (a) with thick interalveolar septum (Is), apparent increased numbers of interstitial cells (Ic) with variable shaped nuclei and also different cytoplasmic profiles of type II pneumocytes (PII).* ***(b)*** *A pneumocyte type II appears with indented nucleus (N), another with heterochromatic nucleus (n), empty lamellar bodiese(e) and megamitochondria (M) are observed. Noticed, no microvilli in the surfaces of pneumocytes type II.* ***[scale bar=5 µm, a= 10um]****.*

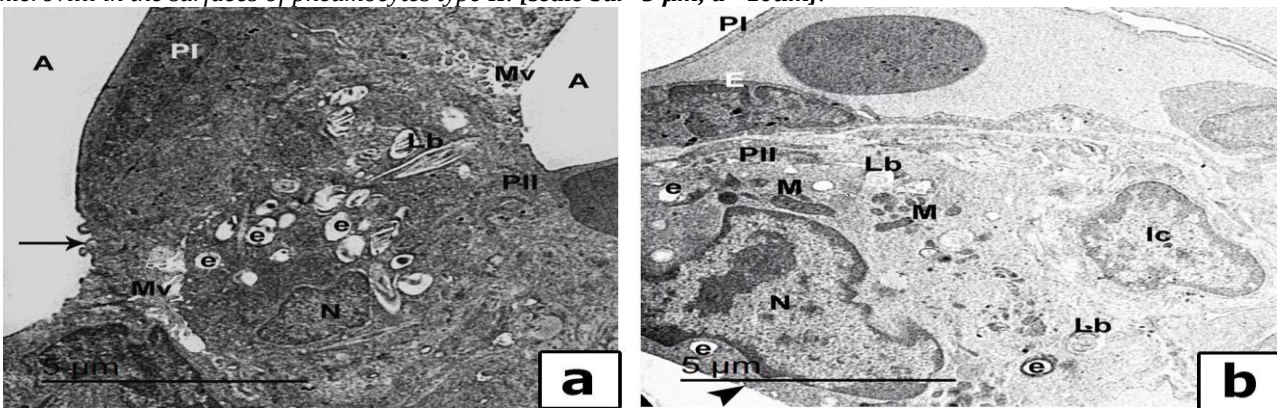

Figure (6): *An electron micrograph of ultrathin sections from the ZnO and ALA-treated group reveals.* ***(a)*** *a part of thick interalveolar septum. It shows a blood capillary with flat indented nucleus (E), thin cytoplasm of type I pneumocyte (PI) and interstitial cell with irregular nucleus (Ic). Type II pneumocyte (PII) showing blunt surface without microvilli (arrow head), indented nucleus with electron dense chromatin (N), characteristic lamellar bodies (Lb), empty lamellar bodies (e), numerous small mitochondria (M) in photo (b) An part of relative thin interalveolar septum between two patent alveoli (A).****(b)*** *shows Type I pneumocyte (PI) lining the alveolar cavity with flat nucleus and some irregularity in its cytoplasm (arrow). Type II pneumocyte (PII) appears with numerous microvilli (Mv), indented small nucleus (N), characteristic lamellar bodies (Lb) and multiple empty lamellar bodies (e).*

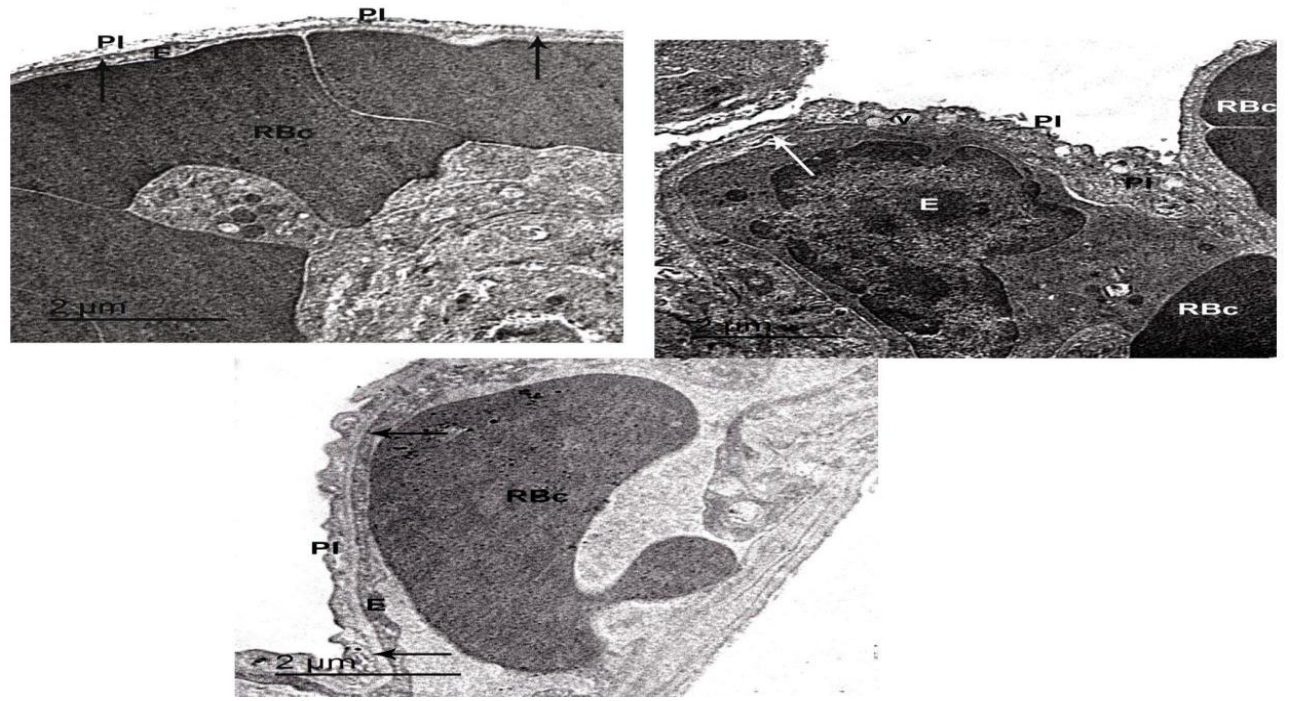

Figure (7): *Representative transmission electron micrographs of ultrathin rat lung sections from various experimental groups, depicting the air-blood barrier: (a) In the control group, the barrier is formed by the attenuated cytoplasm of pneumocyte type I (PI), a thin fused basal lamina (arrow), and the cytoplasm of the capillary endothelial cell (E) with a red blood cell (RBC) in its lumen. (b) In the ZnO group, the air-blood barrier is deformed. It appears with extensive swollen cytoplasm of type I pneumocyte* ***(PI),*** *multiple cytoplasmic vacuoles* ***(v)*** *and thick irregular fused basal lamina* ***(arrow).*** *Capillary endothelium shows an indented nucleus with electron dense chromatin (E) red blood cells* ***(RBc)*** *in its lumen.in (c) Lung of ALA&ZNO recipient group reveals nearly normal air-blood barrier. It appears with thin fused basal lamina* ***(arrow)*** *and little irregular swelling in cytoplasm of both type I pneumocyte* ***(PI)*** *and capillary endothelial cell* ***(E)****. Red blood cell* ***(RBCs)*** *in its lumen is noticed.*

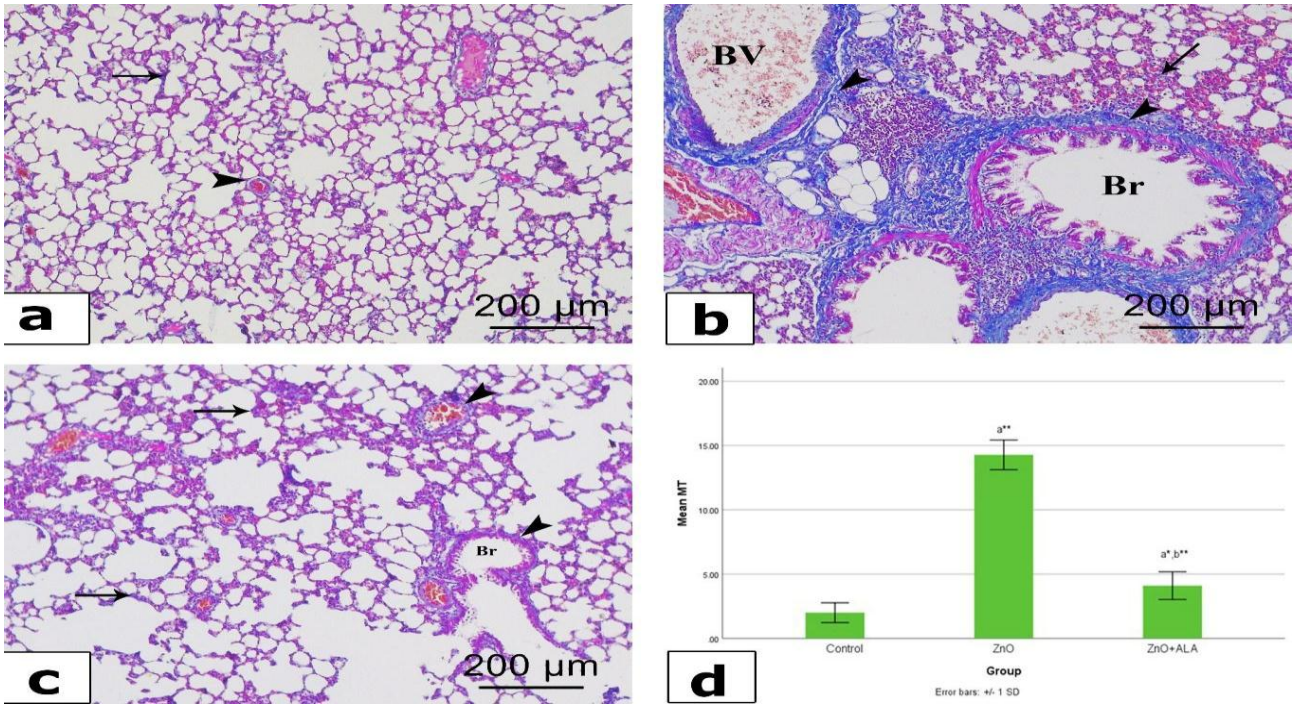

Figure (8): *Representative microscopic images of Mallory's trichrome-stained lung sections from the different experimental groups: a. Control, b. ZnO, and c. ZnO+ALA groups. The arrowhead indicates the blue staining of collagen fibers around the bronchioles (Br) and pulmonary blood vessels (bv), while the arrow points to the blue staining of collagen fibers within the lung interstitium. d) A chart shows the analysis of changes in the percentage area of collagen fiber dispersion across the various groups. Data are presented as means ± standard error of the mean (SEM) and were analyzed using one-way ANOVA followed by Tukey's multiple comparisons test. A level of probability (P value) ≤0.05 was considered significant.* *******Compared with the Control group,* ***#*** *compared with ZNO group.*

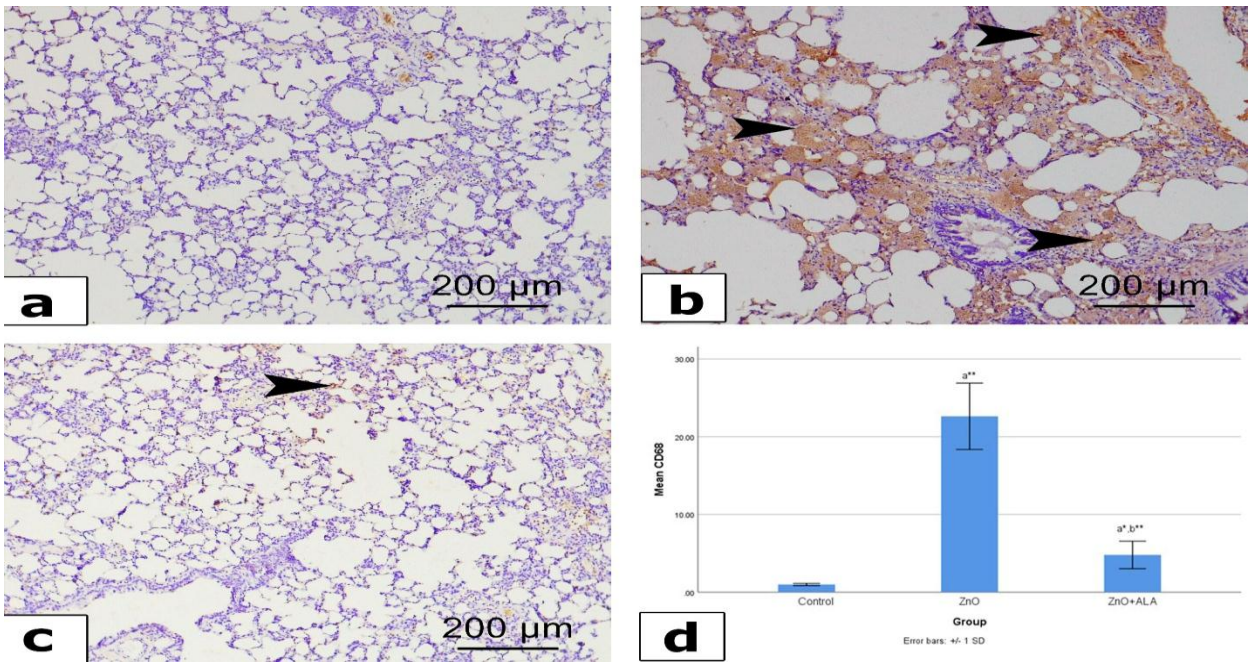

Figure (9): *Representative microscopic images of lung sections immunohistochemically stained with anti-CD68 antibody, highlighting alveolar macrophages from the different experimental groups. a. Control, b. ZNO and c. ZNO+ALA groups. Arrowhead refers to positive brown cytoplasmic reacted cells. d. Histogram shows the statistical analysis of the changes in the % area of CD68 immuno-expression from the different experimental groups* ***[50 µm x400].*** *Data are provided as means with standard error of mean (SEM) and analysed using one-way ANOVA followed by Tukey's multiple comparisons test. A level of probability (P value) ≤0.05 was considered significant.* *******Compared with the Control group, # compared with ZNO group.*

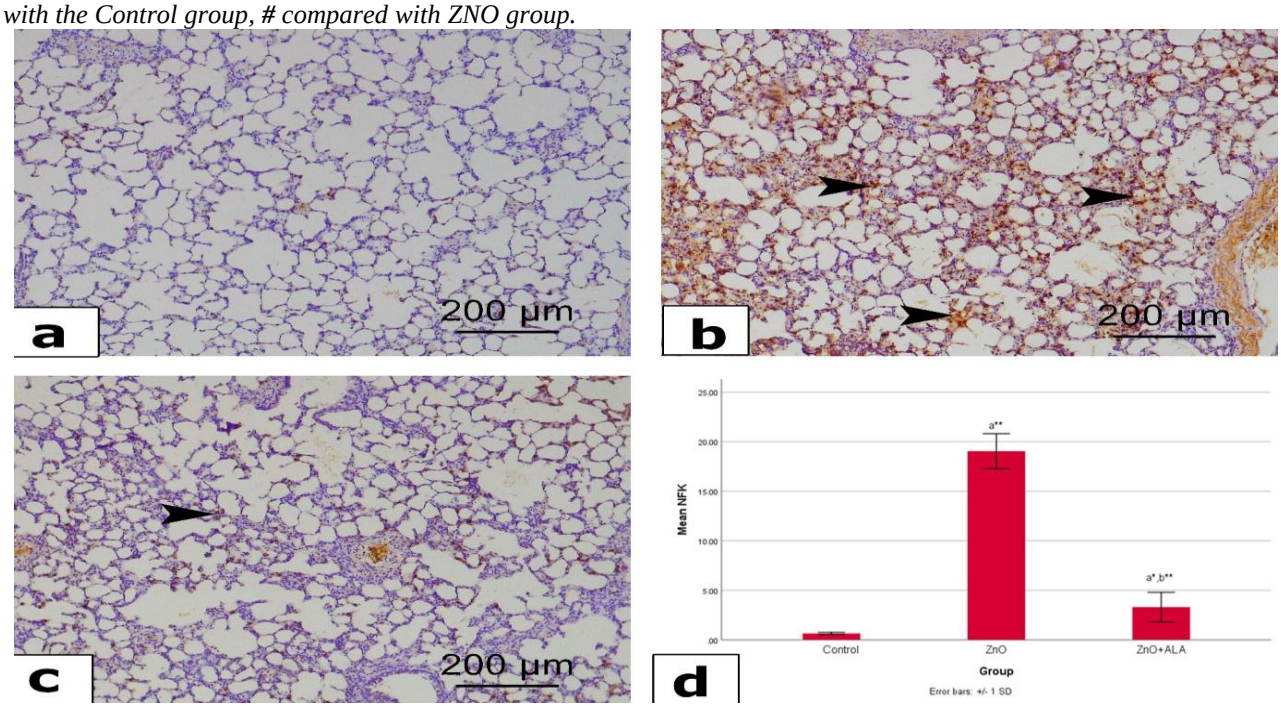

Figure (10): *Repres entative microscopic images of immunohistochemically stained lung sections with NF-κB antibody from different experimental groups. a. Control, b. ZNO and c. ZNO+ALA groups. Arrowhead refers to the brown coloration of the immunopositive cells. d. The histogram shows the quantitative and statistical analysis of the changes in the % area of NF-κB immunopositive cells from the different experimental groups* ***[50 µm x400].*** *Data are provided as means with standard error of mean (SEM) and analysed using one-way ANOVA followed by Tukey's multiple comparisons test. A level of probability (P value) ≤0.05 was considered significant.* *******Compared with the Control group, # compared with ZNO group.* ***Representative microscopic images of lung sections immunohistochemically stained for NF-κB are presented for the various experimental groups:*** *(a) Control, (b) ZnO-treated, and (c) ZnO+ALA-treated groups. Arrowheads indicate immune-positive cells characterized by brown staining* ***[50 µm x400]. (d)*** *The accompanying histogram illustrates the quantitative and statistical evaluation of the percentage area occupied by NF-κB-positive cells across the groups, viewed at 400× magnification with a scale bar of 50 µm. Data are expressed as mean ± standard error of the mean (SEM) and were analysed using one-way ANOVA followed by Tukey's post hoc multiple comparisons test. A P-value ≤ 0.05 was considered statistically significant.*

DISCUSSION

Zinc oxide nanoparticles (ZnO-NPs) are considered one of the commonly utilized NPs, with the respiratory system reported as the chief route for entry ***(Choi and Choy, 2014; Al-Ali et al., 202)***. However, wide variation in ZnO-NPs toxicity was reported, which depends on various factors like size, dose, route of administration, as well as duration of exposure ***(Lee et al., 2013)***.

Existing literature indicates that exposure to ZnO-NPs in the lungs triggers a strong inflammatory response in the initial stages. Studies in rats treated with ZnO-NPs have generally reported elevated levels of various cytokines, with interleukin-6 (IL-6) in addition to tumor necrosis factor-alpha (TNF-α) being particularly affected, thereby promoting the infiltration of granulocytes ***(Jung et al., 2021)***.

Inhalation of 0.5 mg/m³ ZnO-NPs caused airway inflammation, along with elevated protein levels of IL-6 and IL-8, and an increased neutrophil count in sputum ***(Monsé et al., 2019)***. Therefore, the aim of this study was to evaluate the protective roles of ALA for rats exposed to zinc oxide nanomaterials on lung tissue by assessing the level of different biochemical markers in the lung homogenate, in addition to assessing gene expression of different parameters of tissue oxidation, inflammation, damage, and apoptosis.

By biochemical testing, it was found that the level of Superoxide Dismutase (SOD); a very important antioxidant ***(Younus, 2018)***, and Glutathione peroxidase 1 (GPX1); an important cellular antioxidant enzyme ***(Handy and Loscalzo, 2022)*** in the lung tissues of the protective group who received intraperitoneal (IP) injection of Zinc oxide nanoparticles in addition to alpha lipoic acid showed higher levels than in the lung tissues of the treated group who received intraperitoneal (IP) injection of Zinc oxide nanoparticles only. In addition, the measured lung tissue levels of Malondialdehyde (MDA); a lipid peroxidation biomarker ***(Gawel et al., 2004)***; Tumor necrosis factor alpha (TNF –α); an inflammatory cytokine ***(Idriss and Naismith, 2000)***, and Interleukin–6 (IL 6); a cytokine produced in response to tissue damage ***(Tanaka et al., 2014)*** were lower in the protective group than in the treated group who received ZnO-NPs only).

Oxidative and inflammatory mediators are known to contribute to tissue damage since they can react with DNA molecules causing strand breaks and damage which subsequently trigger cell apoptosis via mediating signal transducers ***(Lee et al., 2016)***. Consistent with our results, Oxidative stress is recognized as a key factor in metal-induced toxicity, where the imbalance between free radicals and antioxidants like SOD and GPX leads to oxidative damage and, ultimately, organ toxicity ***(Ighodaro and Akinloye, 2018)***. A study found that an increase in the nervous, immune, and male reproductive systems' oxidative stress was observed in lead- and ZnO-NP-exposed groups of animals. Moreover, when treated with ALA, reduction in the induced oxidative stress was detected, which suggested its antioxidant potential in addition to reduced levels of apoptotic caspase-3 in both spleen and brain tissues, suggesting its anti-apoptotic effect in those organs. Finally, a metal chelating property of ALA was reported ***(Deore et al., 2021)***.

Although In vitro and in vivo studies have yielded inconsistent results regarding the effects of ALA supplementation on nanomaterial-induced oxidative and inflammatory damage, its beneficial impact and the recommendation for its oral use in preventing and treating various oxidative and inflammation-related diseases have been well-documented ***(Luo et al., 2022)***. In addition, the literature indicates the potential of ALA in mitigating metal-induced toxicity ***(Deore et al., 2021)***.

As regards gene expression analysis of Transforming growth factor beta (TGF-β), a crucial factor in cell proliferation, differentiation, and apoptosis ***(Morikawa et al., 2016)***, Natural cytotoxicity triggering receptor 3 (Ncr3) gene; the gene for the natural cytotoxicity triggering receptors ***(Kruse et al., 2014)***, SMAD2, SMAD3, both are protein-coding genes which are important in mediating TGF-β signals ***(Massagué et al., 2005)***. Matrix metalloproteinase 9 (MMP9), a member of zinc-dependent endopeptidases ***(Vandooren et al., 2013)***, collagen type I (Col

1A1), the fibrillar collagen gene most commonly associated with disease ***(Viguet-Carrin et al., 2006)***. Fibronectin, a multifunctional adhesive glycoprotein with critical role in tissue repair ***(To and Midwood, 2011)***, monocyte chemoattractant protein-1(MCP1); an essential chemokine which plays a pivotal role in inflammation and other diseases ***(Singh et al., 2021)***, all of those genes show significantly lower expression level in the protective group than in the treated group who received ZnO-NPs only.

As regards Mothers against decapentaplegic homolog 7 (SMAD7); a gene coding for a protein which has protective roles on fibrotic damage through preventing TGF-induced extracellular matrix production ***(Singh et al., 2021)*** and Il-10; a powerful anti-inflammatory cytokine ***(Saraiva et al., 2019)***. It was found that the treated group that received ZnO-NPs had a significantly lower level than all other experimental groups. Furthermore, the protective group, which received additional alpha lipoic acid, had a significantly lower level than the experimental control. These findings support a study that investigated the therapeutic potential of (ZnO-ALA) nanoparticles in cardiovascular stent, as poly (L-lactic acid) (PLLA) scaffold including synthesized ZnO-ALA nanoparticles revealed promising effects such as suppressing platelet adhesion and activation, augmenting proliferation of endothelial cells, and reducing growth of smooth muscle cells, suggesting excellent angiogenic and anti-inflammatory effects of those nanoparticles ***(Baek et al., 2023)***.

The effect of ZnO-NP on lung tissues was accompanied by histopathological alteration. The histopathological alterations found in the lung sections of the ZnO-NP-treated group were in agreement with other studies. ***Mohammed et al. (2022)*** reported that, alveolar damage characterized by collapsed alveoli, thickened interalveolar septa, in addition to bronchial walls with dense infiltration of inflammatory cells and thickened vascular walls. Similarly, ***Junge et al. (2021)*** observed neutrophilic infiltration in alveolar and bronchoalveolar regions following ZnO-NP exposure, contributing to increased alveolar wall thickness. Furthermore, pulmonary lesions associated with ZnO-NP toxicity, including serous inflammation, severe alveolar hyperemia, and edema, have been documented. Another study reported that a single pulmonary exposure to 6 mg ZnO-NPs (0.3 mg/kg body weight) led to acute inflammation, extensive epithelial cell desquamation, alveolar barrier disruption, epithelial proliferation, and edema ***(Jacobsen et al., 2015)***.

Wang et al. (2017) further demonstrated that intratracheal instillation of ZnO-NPs (200–800 μg/kg) induced inflammatory and hyperplastic lung changes. The detected pulmonary hyperplasia in our study likely resulted in impaired gas exchange due to alveolar wall thickening, along with hypertrophic changes in smooth muscle fibers and blood vessels caused by increased extracellular protein deposition. Additionally, the pulmonary congestion noted in this study may reflect vascular hypertension or impaired blood flow ***(Al-Ali et al., 2022)***.

Zinc oxide nanoparticle toxicity is predominantly attributed to increased ROS generation, resulting in genotoxicity, inflammation, and cell death ***(Attia et al., 2018)***. Our results demonstrated significant fibrosis in ZnO-NP-exposed lung tissue, characterized by increased collagen deposition around bronchioles, pulmonary blood vessels, and interstitial spaces, consistent with the findings of ***Mohammed et al. (2022)***. Normally, collagen fibers in alveolar walls are sparse and cannot be detected except by electron microscopy. Thus, their presence under routine light microscopy suggests pathological fibrosis. Ultrastructural analysis in the current study further confirmed these findings, revealing thickened interalveolar septa, congested blood capillaries, and deformed air-blood barriers, with swollen pneumocyte type I cells and capillary endothelial cells, which are similar to observations by ***(Morimoto et al. 2016; Oyabu et al., 2017)***. Inflammatory responses induced by ZnO-NPs were evidenced by a significant increase in CD68-positive macrophages within alveolar spaces, aligning with ***Mohamed et al. (2022)*** who reported a marked rise in CD68-positive immunoreactive cells following Ag-NP

exposure. This macrophage activation is likely a compensatory response to counteract the inflammatory cascade and oxidative stress triggered by nanoparticle exposure. Macrophages play a pivotal role in nanoparticle clearance, with Ag-NPs eliciting a stronger macrophage response compared to TiO_2-NPs ***(Gawish et al., 2018)***.

Additionally, our findings showed significantly elevated NF-κB immuno-expression in ZnO-NP-treated lungs, consistent with ***Fan et al. (2015)***, reinforcing the role of NF-κB in mediating nanoparticle-induced inflammation. Alpha-lipoic acid (ALA) treatment effectively mitigated ZnO-NP-induced lung injury by reducing oxidative stress, inflammation, and fibrosis, as supported by histopathological improvements in ALA-treated rats. Notably, ALA significantly decreased collagen accumulation by 30.3% compared to the ZnO-NP-treated group, in agreement with ***Ibrahim et al. (2021)***. These findings align with many studies confirming ALA's antioxidant and cytoprotective properties ***(Lin et al., 2013; Arpag et al., 2018)***. The observed reduction in collagen deposition following ALA treatment suggests its potential anti-fibrotic role, likely mediated by its antioxidant capabilities ***(Antar et al., 2023)***. Biochemical analysis further corroborated the protective effects of ALA, demonstrating a significant decline in MDA levels and an increase in antioxidant enzyme activity, particularly SOD ***(Ak et al., 2023)***. ALA enhances the cellular antioxidant defense system by boosting glutathione (GSH), GPX, SOD, and catalase (CAT) levels, thereby neutralizing ROS and promoting cellular survival. Uniquely, ALA not only acts as a potent antioxidant but also enhances mitochondrial energy metabolism as a cofactor for respiratory enzymes ***(Ramos et al., 2023)***. Additionally, ALA has been reported to reduce apoptosis induced by oxidative stress and protect cellular redox homeostasis ***(Jeffrey et al., 2021)***.

CONCLUSION

This study demonstrated that alpha-lipoic acid (ALA) provides significant protective effects against zinc oxide nanoparticle (ZnO-NP)-induced pulmonary toxicity in rats. The administration of ALA effectively mitigated oxidative stress by increasing antioxidant enzyme levels (SOD, GPX1) and reducing lipid peroxidation (MDA). Additionally, ALA attenuated inflammation by lowering TNF-α and IL-6 levels while modulating fibrosis-related gene expression, reducing the expression of TGF-β1, Ncr3, SMAD2, SMAD3, MMP9, Col 1A1, Fibronectin, and MCP-1, and upregulating the anti-inflammatory and antifibrotic markers SMAD7 and IL-10. Histopathological analysis further confirmed that ALA preserved lung tissue integrity by reducing cellular damage and apoptosis. These findings highlight ALA's potential as a protective agent against ZnO-NP-induced lung toxicity, suggesting its possible therapeutic application in preventing nanoparticle-related pulmonary damage. Further studies are recommended to explore its clinical relevance and optimal dosing strategies.

Authors' contributions:

Amira Ebrahim Alsemeh, on behalf of the co-authors, confirms the originality and integrity of this study, which investigates the protective effects of alpha-lipoic acid (ALA) against zinc oxide nanoparticle (ZnO-NP)-induced pulmonary toxicity in rats. By assessing oxidative stress markers, inflammatory cytokines, gene expression of fibrosis and immune response markers, as well as histopathological and ultrastructural lung alterations, this study provides novel insights into the ameliorative potential of ALA. The findings demonstrate that ALA effectively mitigates ZnO-NP-induced lung toxicity by reducing oxidative stress, inflammation, and fibrosis-related gene expression. We collectively confirm compliance with ethical guidelines, institutional acceptance, and declare no conflicts of interest related to this work. We believe this study contributes to a deeper understanding of nanoparticle-induced effects of pulmonary toxicity and underscores ALA as a promising protective agent for future translational and clinical applications.

Declaration of competing interest: The authors have no competing interest to declare.

Funding: This study was conducted without any specific financial support from public, commercial, or nonprofit funding agencies.

Consent for publication: All authors have approved the final article for publication.

Data Availability: Data will be provided upon request.

REFERENCES

1. **Abd el Fadil, H.; Moustafa, A.; khalifa, H. et al. (2020):** Cinnamon extract ameliorates liver damage and oxidative stress induced by paracetamol in male rats. *Damanhour J.Vet. Sci., 3: 12-20.*
2. **Abd El-Galil A. M. and Alkot, A. M. F. (2022):** Impact of crude aloe vera gel on silver nanoparticle-induced lung cytotoxicity in adult male albino rats: functional, histological and immunohistochemical study. *Al-Azhar Med.J., 51: 563-604.*
3. **Ak, E.; Muhan, A.; Çalışkan, S. et al. (2023):** Comparison of the protective effect of alpha lipoic acid and quercetin in methotrexate-induced lung damage. *Bagcilar Med. Bull.,8(1):82:87.*
4. **Al-Ali, A. A.; Al-Tamimi, S. Q.; Al-Maliki, S. J. et al. (2022):** Toxic effects of zinc oxide nanoparticles and histopathological and Caspase-9 expression changes in the liver and lung tissues of male mice model. *App.Nanosci., 1-11.*
5. **Amendola, V.; Amans, D.; Ishikawa, Y. et al. (2020):** Room-temperature laser synthesis in liquid of oxide, metal-oxide core-shells, and doped oxide nanoparticles. *Chem. Euro. J.,* 26*: 9206-9242.*
6. **Anjum, S.; Hashim, M.; Malik, S. A. et al. (2021):** Recent advances in zinc oxide nanoparticles (zno nps) for cancer diagnosis, target drug delivery, and treatment. *Cancers, 13: 4570.*
7. **Ansari, M. A.; Khan, H. M.;Khan, A. A. et al. (2015):** Biochemical and histopathological ultrastructural changes caused by ZnO nanoparticles in mice. *Toxicol. Environ.Chem., 97: 1025-1040.*
8. **Antar, S. A.; Ashour, N. A.; Marawan, M. E. et al. (2023):** Fibrosis: Types, effects, markers, mechanisms for disease progression, and its relation with oxidative stress, immunity, and inflammation. *Int. J. Molec. Sci., 24: 4004.*
9. **Arpag, H.; Gül, M.; Aydemir, Y. et al. (2018):** Protective effects of alpha-lipoic acid on methotrexate-induced oxidative lung injury in rats. *J. Invest. Surg., 31: 107-113.*
10. **Attia, H., Nounou, H. and Shalaby, M. (2018):** Zinc oxide nanoparticles induced oxidative dna damage, inflammation, and apoptosis in rats'brains after oral exposure. *Toxics, 29:6.*
11. **Baek, S. W.; Kim, D. S.; Lee, J. K. et al. (2023):** Continuous dual-generation by ZnO nanoparticle conjugated with α-lipoic acid for functional biodegradable vascular stent. *Chem. Eng. J., 470: 144174.*
12. **Castro, M. C.; Villagarcía, H. G.; Massa, M. L. et al. (2019):** Alpha-lipoic acid and its protective role in fructose-induced endocrine-metabolic disturbances. *Food Function, 10: 16-25.*
13. **Chen, Y. Y.; Lee, Y. H.; Wang, B.J. et al. (2022):** Skin damage induced by zinc oxide nanoparticles combined with UVB is mediated by activating cell pyroptosis via the NLRP3 inflammasome–autophagy–exosomal pathway. *Particle Fibre Toxicol.,19: 1-22.*
14. **Choi, S. J. and Choy, J. H. (2014):** Biokinetics of zinc oxide nanoparticles: toxicokinetics, biological fates, and protein interaction. *Int. J. Nanomed., 9: 261-269.*
15. **Czyżowska, A. and Barbasz, A. (2022):** A review: Zinc oxide nanoparticles–friends or enemies? *Int. J. Environ. Health Res., 32: 885-901.*
16. **Deore, M. S. K.; Naqvi, S.; Kumar, A. et al. (2021):** Alpha-lipoic acid protects against co-exposure to lead and zinc oxide nanoparticles induced neuro, immuno, and male reproductive toxicity in rats. *Front. Pharmacol., 12: 626238.*
17. **Fan, Z.; Yao, J.; Li, Y. et al. (2015):** Anti-inflammatory and antioxidant effects of curcumin on acute lung injury in a rodent model of intestinal ischemia reperfusion by inhibiting the pathway of nf-kb. *Int. J. Clin. Eexp. Pathol.,8:3451.*
18. **Fenga, C.; Gangemi, S.; Di Salvatore, V. et al. (2017):** Immunological effects of occupational exposure to lead. *Molec. Med. Rep., 15: 3355-3360.*
19. **Fouad, H.; Yang, G.; El-sayed, A. A. et al. (2021):** Green synthesis of agnp–ligand complexes and their toxicological effects on nilaparvata lugens. *J. Nnanobiotechnol., 19:1-17.*
20. **Gaweł, S.; Wardas, M.; Niedworok, E. et al. (2004):** Malondialdehyde (MDA) as a lipid peroxidation marker. *Wiadomosci lekarskie (warsaw, poland: 1960), 57: 453-455.*
21. **Gawish, M.; Shaban,S.; Abdel Aal, S. et al. (2018):** Effect of silver nanoparticles versus titanium dioxide nanoparticles on the lung of adult male albino rats: a histological and

immunohistochemical study. *J. Med. Histol., 2: 181-200.*

22. **Guo, T.; Fang, X.; Liu, Y. et al. (2022):** Acute lung inflammation induced by zinc oxide nanoparticles: Evolution and intervention via NRF2 activator. *Food Chem. Toxicol., 162: 112898.*
23. **Handy, D. E. and Loscalzo, J. (2022):** The role of glutathione peroxidase-1 in health and disease. *Free Rad. Biol. Med.,* 188*: 146-161.*
24. **Hayat, M. A. (1973):** Principles and techniques of electron microscopy. *Biol. Aapp., 3*
25. **Henriksen, E. J. (2006):** Exercise training and the antioxidant α-lipoic acid in the treatment of insulin resistance and type 2 diabetes. *Free Rad. Biol.Med,* 40*: 3-12.*
26. **Ibrahim, G. R. and Mousa, M. (2021):** The protective potential of alpha lipoic acid on amiodarone-induced pulmonary fibrosis and hepatic injury in rats. *Molec. Cell. Biochem., 476: 3433-3448.*
27. **Idriss, H. T. Naismith, J. H. (2000):** TNFα and the TNF receptor superfamily: structure-function relationship (s). *Microscopy Res. Tech., 50:184-195.*
28. **Ighodaro, O. and akinloye, O. (2018):** First line defence antioxidants-superoxide dismutase (sod), catalase (cat) and glutathione peroxidase (gpx): Their fundamental role in the entire antioxidant defence grid. *Alexandria J. Med., 5**4**: 287-*293.
29. **Jacobsen, N. R.; Stoeger, T.; Van den Brûle, S. et al. (2015):** Acute and subacute pulmonary toxicity and mortality in mice after intratracheal instillation of ZnO nanoparticles in three laboratories. *Food Chem.Toxicol., 85: 84-95.*
30. **Jan, A. T.; Azam, M.; Siddiqui, K. et al. (2015):** Heavy metals and human health: mechanistic insight into toxicity and counter-defense system of antioxidants. *Int. J. Molec. Ssci.,16: 29592-29630.*
31. **Jeffrey, S.; Samraj, P. I. and Raj, B. S. (2021):** The role of alpha-lipoic acid supplementation in the prevention of diabetes complications: a comprehensive review of clinical trials. *Curr. Diabetes Rev., 17: 87-98.*
32. **Jung, A., Kim, S. H., Yang, J. Y. et al. (2021):** Effect of pulmonary inflammation by surface functionalization of zinc oxide nanoparticles. *Toxics, 9: 336.*
33. **Kad, A.; Pundir, A.; Arya, S. K. (2022):** Meta-analysis of in vitro cytotoxicity evaluation studies of zinc oxide nanoparticles: Paving the way for safer innovations. *Toxicol. In vitro, 83: 105418.*
34. **Keerthana, S. and Kumar, A. (2020):** Potential risks and benefits of zinc oxide nanoparticles: a systematic review. *Crit. Rev. Toxicol., 50:47-71.*
35. **Khamis, T.; Abdelalim, A.; Abdallah, S. et al. (2019):** Breast milk mscs transplantation attenuates male diabetic infertility via an immunomodulatory mechanism in rats. *Adv. Anim. Vet. Sci, 7:145-153.*
36. **Khamis, T.; Abdelalim, A. F.; Abdallah, S. H. et al. (2020):** Early intervention with breast milk mesenchymal stem cells attenuates the development of diabetic-induced testicular dysfunction via hypothalamic kisspeptin/kiss1r-gnrh/gnih system in male rats. *Biochim. Biophys. Acta (BBA), 866: 165577.*
37. **Khamis, T.; Abdelalim, A. F.; Saeed, A. A. et al. (2021):** Breast milk MSCs upregulate β-cells pdx1, ngn3, and pcna expression via remodeling er stress/inflammatory/ apoptotic signaling pathways in type 1 diabetic rats. *Euro.J. Pharmacol., 905: 174188.*
38. **Kruse, P. H.; Matta, J.; Ugolini, S. et al. (2014):** Natural cytotoxicity receptors and their ligands. *Immunol. Cell Biol., 92: 221-229.*
39. **Lee, J.; Kim, Y.; Lim, S. et al. (2016):** Single-molecule visualization of ROS-induced DNA damage in large DNA molecules. *Analyst,* 141*: 847-852.*
40. **Lee, J. H.; Kim, Y. S.; Song, K. S. et al. (2013):** Biopersistence of silver nanoparticles in tissues from Sprague–Dawley rats. *Particle Fibre Toxicol.,10: 1-14.*
41. **Lin, Y. C., Lai, Y. S. and Chou, T.C. (2013):** The protective effect of alpha-lipoic Acid in lipopolysaccharide-induced acute lung injury is mediated by heme oxygenase-1. *Evid. Based Comp. Altern. Med., 2013, 590363*
42. **Livak, K. J. and Schmittgen, T. D. (2001):** Analysis of relative gene expression data using real-time quantitative PCR and the 2-ΔΔct method. *Methods,* 25*: 402-408.*
43. **Luo, X.; Xie, D.; Wu, T. et al. (2022):** Evaluation of the protective roles of alpha-lipoic acid supplementation on nanomaterial-induced toxicity: A meta-analysis of in vitro and in vivo studies. *Front. Nutr., 9: 991524.*

44. **Mohammed, H. A.. L.; El shakaa, N. M.; Bahaa, N. et al. (2022):** A histological study on the acute effect of zinc oxide nanoparticles administered by different routes on albino rat lung. *J. Microscopy Ultrastr., 10: 72-80.*
45. **Monsé, C.; Raulf, M. ; Hagemeyer, O. et al. (2019):** Airway inflammation after inhalation of nano-sized zinc oxide particles in human volunteers. *BMC Pulm. Med., 19: 1-11.*
46. **Morikawa, M.; Derynck, R. and Miyazono, K. (2016):** TGF-B and the TGF-B family: Context-dependent roles in cell and tissue physiology. *Cold Spring Harbor Persp. Biol.8:a021873.*
47. **Mozaffari, Z.; Parivar, K.; Roodbari, N. H. et al. (2015):** Histopathological evaluation of the toxic effects of zinc oxide (ZnO) nanoparticles on testicular tissue of NMRI adult mice. *Adv. Stud. Biol., 7: 275-291.*
48. **Oyabu,T.; Myojo, T.; Lee, B. W. et al. (2017):** Biopersistence of NiO and TiO2 nanoparticles following intratracheal instillation and inhalation. *Int. J. Molec. Sci., 18: 2757..*
49. **Packer, L. and Cadenas, E. (2010):** Lipoic acid: Energy metabolism and redox regulation of transcription and cell signaling. *J. Clin. Biochem. Nutr.,48:26-32.*
50. **Ramos-Vara, J. A. (2010):** Principles and Methods of Iimmunohistochemistry. *Drug safety evaluation: Methods and protocols, p.p.83-96.*
51. **Ramos, C. S. C.; Silva, V. A. P. D.; Corrêa, L. B. N. S. et al. (2023):** Long-term alpha-lipoic acid) ALA) antioxidant therapy reduces damage in the cardiovascular system of streptozotocin-induced diabetic rats. *J. Diet. Supp., 20: 444-458.*
52. **Rasheed, N. A.; Abdel Baky, N.; Shebly, W. et al. (2012):** Effect of vitamin E and α-lipoic acid on nano zinc oxide-induced renal cytotoxicity in rats. *Afr. J. Pharm. Pharmacol., 6: 2211-2223.*
53. **Rogers, L. K. and Cismowski, M. J. (2018):** Oxidative stress in the lung–the essential paradox. *Curr. Opin. Ttoxicol.7:37-43.*
54. **Salehi, B.; Berkay Yılmaz, Y.; Antika, G. et al. (2019):** Insights on the use of α-lipoic acid for therapeutic purposes. *Biomolec.,9: 356.*
55. **Sanderson, T.; Wild, G.; Cull, A . M. et al. (2018):** Immunohistochemical and 19 immunofluorescent techniques. *Bancroft's Theory and Practice of Histological Techniques e-book, p.p.337.*
56. **Saraiva, M.; Vieira, P. and O'garra, A. (2019):** Biology and therapeutic potential of interleukin-10. *J. Exp. Med., 217: e20190418.*
57. **Singh, S.; Anshita, D. and Ravichandiran, V. (2021):** MCP-1: function, regulation, and involvement in disease. *Int. Immunopharmacol.,101: 107598.*
58. **Suvarna, K. S.; Layton, C. and Bancroft, J. D. (2018):** *Bancroft's Theory and Practice of Histological Techniques e-book, Elsevier Health Sciences.*
59. **Tanaka, T.; Narazaki, M. and Kishimoto, T. (2014):** IL-6 in inflammation, immunity, and disease. *Cold Spring Harbor Persp. Biol.*, 6, *a01629.*
60. **Taylor, C. R. (2014):** Immunohistochemistry in surgical pathology: principles and practice. *Histopathol. Methods Protocols,p.p.81-109.*
61. **To, W. S. and Midwood, K. S. (2011):**Plasma and cellular fibronectin: Distinct and independent functions during tissue repair. *Fibrogen. Tiss.Repair, 4:1-17.*
62. **Vandooren, J. ; Van den Steen, P. E. and Opdenakker, G. (2013):** Biochemistry and molecular biology of gelatinase b or matrix metalloproteinase-9 (MMP-9): The next decade. *Crit. Rev. Biochem.Molc. Biol.48: 222272.*
63. **Vasantharaj, S.; Sathiyavimal, S. ; Senthilkumar, P. et al. (2021):** Enhanced photocatalytic degradation of water pollutants using bio-green synthesis of zinc oxide nanoparticles (zno nps). *J. Environ.Chem. Eng.*, 9: 105772.
64. **Viguet-carrin, S.; Garnero, P. and Delmas, P. (2006):** The role of collagen in bone strength. *Osteoporosis Int., 17: 319-336.*
65. **Wang, D.; Li, H.; liu, Z. et al. (2017):** Acute toxicological effects of zinc oxide nanoparticles in mice after intratracheal instillation. *Int. J. Occup. Environ. Health, 23: 11-19.*
66. **Wesselink, E.; Koekkoek, W.; Grefte, S. et al. (2019):** Feeding mitochondria: potential role of nutritional components to improve critical illness convalescence. *Clin. Nutr., 38:982-995.*
67. **Younus, H. (2018):** Therapeutic potentials of superoxide dismutase. *Int. J. Health Sci., 12:88.*